

# Extreme rainfall activity in the Australian tropics reflects changes in the El Niño/Southern Oscillation over the last two millennia

Rhawn F. Denniston<sup>a,1</sup>, Gabriele Villarini<sup>b</sup>, Angelique N. Gonzales<sup>a</sup>, Karl-Heinz Wyrwoll<sup>c</sup>, Victor J. Polyak<sup>d</sup>, Caroline C. Ummenhofer<sup>e</sup>, Matthew S. Lachniet<sup>f</sup>, Alan D. Wanamaker Jr.<sup>g</sup>, William F. Humphreys<sup>h</sup>, David Woods<sup>i</sup>, and John Cugley<sup>j</sup>

<sup>a</sup>Department of Geology, Cornell College, Mount Vernon, IA 52314; <sup>b</sup>IHR-Hydroscience & Engineering, University of Iowa, Iowa City, IA 52240; <sup>c</sup>School of Earth and Environment, University of Western Australia, Crawley, WA 6009, Australia; <sup>d</sup>Department of Earth and Planetary Sciences, University of New Mexico, Albuquerque, NM 87131; <sup>e</sup>Department of Physical Oceanography, Woods Hole Oceanographic Institution, Woods Hole, MA 02543; <sup>f</sup>Department of Geoscience, University of Nevada, Las Vegas, NV 89154; <sup>g</sup>Department of Geological and Atmospheric Sciences, Iowa State University, Ames, IA 50011; <sup>h</sup>Western Australia Museum, Welshpool DC, WA 6986, Australia; <sup>i</sup>Department of Parks and Wildlife, Broome, WA 6725, Australia; and <sup>j</sup>Australian Speleological Federation, Willetton, WA 6155, Australia

Edited by Kerry A. Emanuel, Massachusetts Institute of Technology, Cambridge, MA, and approved March 10, 2015 (received for review November 20, 2014)

**Assessing temporal variability in extreme rainfall events before the historical era is complicated by the sparsity of long-term “direct” storm proxies. Here we present a 2,200-y-long, accurate, and precisely dated record of cave flooding events from the northwest Australian tropics that we interpret, based on an integrated analysis of meteorological data and sediment layers within stalagmites, as representing a proxy for extreme rainfall events derived primarily from tropical cyclones (TCs) and secondarily from the regional summer monsoon. This time series reveals substantial multicentennial variability in extreme rainfall, with elevated occurrence rates characterizing the twentieth century, 850–1450 CE (Common Era), and 50–400 CE; reduced activity marks 1450–1650 CE and 500–850 CE. These trends are similar to reconstructed numbers of TCs in the North Atlantic and Caribbean basins, and they form temporal and spatial patterns best explained by secular changes in the dominant mode of the El Niño/Southern Oscillation (ENSO), the primary driver of modern TC variability. We thus attribute long-term shifts in cyclogenesis in both the central Australian and North Atlantic sectors over the past two millennia to entrenched El Niño or La Niña states of the tropical Pacific. The influence of ENSO on monsoon precipitation in this region of northwest Australia is muted, but ENSO-driven changes to the monsoon may have complemented changes to TC activity.**

tropical cyclone | ENSO | flood | stalagmite | Australia

Two primary components of tropical precipitation—monsoons and tropical cyclones (TCs)—are capable of producing high volumes of rainfall in short periods of time (extreme rainfall events) that lead to flooding. Because both systems respond to changes in atmospheric and sea surface conditions (1, 2), it is imperative that we understand their sensitivities to climate change. For example, over recent decades, warming of the oceans has driven increases in the mean latitude (3) and energy released by TCs (4). These storms (e.g., hurricanes, typhoons, tropical storms, and tropical depressions) can produce enormous economic and societal disruptions but also represent important components of low-latitude hydroclimate (5) and ocean heat budgets (6). Monsoon reconstructions spanning the last several millennia have been developed using a variety of proxies (7–10), including stalagmites (11–13), but reconstructing past TC activity is generally more difficult. In most of the world’s ocean basins, accurate counts of TCs are limited to the start of the satellite era (since 1970 CE), an interval too short to capture changes occurring over multidecadal to centennial time scales. Therefore, as a complement to the historical record, sedimentological analyses of storm-sensitive sites have formed the basis of TC reconstructions, primarily in and around the North Atlantic and Caribbean basins (14–19), that largely focus on near-coastal

sequences, including beach ridges, overwash deposits, and shallow marine sediments. Together, these studies have revealed that North Atlantic and Caribbean TC activity varied substantially over the past several centuries to millennia, with multicentennial shifts attributed to a range of factors including atmospheric dynamics in the North Atlantic, North African rainfall, and El Niño/Southern Oscillation (ENSO).

Today, ENSO represents a dominant control of interannual TC activity at a global scale through its influences on surface ocean temperature gradients and atmospheric circulation (20–23). However, no record has clearly demonstrated the link between ENSO and prehistoric TCs in the tropical Pacific, Indian, or Australian regions, leaving unanswered questions about the sensitivity of cyclogenesis to ENSO before the modern era. This issue is of particular concern given modeling results that predict changes in ENSO behavior may accompany anthropogenic warming of the atmosphere (24, 25). Fully assessing the sensitivity of TCs to changes in climate requires high-resolution and precisely dated paleostorm reconstructions from multiple basins spanning periods beyond those available in observational data, a goal that has largely proven elusive.

## Significance

Variations in tropical cyclone (TC) activity are poorly known prior to the twentieth century, complicating our ability to understand how cyclogenesis responds to different climate states. We used stalagmites to develop a near-annual record of cave flooding from the central Australian tropics, where TCs are responsible for the majority of extreme rainfall events. Our 2,200-year time series reveals shifts in the mean number of storms through time, similar to TC variability from the North Atlantic. This finding is consistent with modern relationships between El Niño/Southern Oscillation (ENSO) and cyclogenesis, as well as with the reconstructed state of ENSO over the past two millennia, suggesting that changes between La Niña- and El Niño-dominated periods drove multicentennial shifts in TC activity in both basins.

Author contributions: R.F.D. and K.-H.W. designed research; R.F.D., V.J.P., M.S.L., A.D.W., W.F.H., D.W., and J.C. performed research; R.F.D., G.V., A.N.G., V.J.P., C.C.U., M.S.L., and A.D.W. analyzed data; and R.F.D., G.V., A.N.G., K.-H.W., V.J.P., C.C.U., M.S.L., A.D.W., and W.F.H. wrote the paper.

The authors declare no conflict of interest.

This article is a PNAS Direct Submission.

Data deposition: The KNI-51 flood layer time series have been published on the NOAA Paleoclimate website, [www.ncdc.noaa.gov](http://www.ncdc.noaa.gov).

<sup>1</sup>To whom correspondence should be addressed. Email: [rdenniston@cornellcollege.edu](mailto:rdenniston@cornellcollege.edu).

This article contains supporting information online at [www.pnas.org/lookup/suppl/doi:10.1073/pnas.1422270112/-DCSupplemental](http://www.pnas.org/lookup/suppl/doi:10.1073/pnas.1422270112/-DCSupplemental).

Few such records unambiguously derived from TCs have been identified, particularly in the western Pacific and Indo-Pacific (20, 26–30).

### Study Area and Conceptual Model

We present a near-annual resolution flood record from cave KNI-51 in the central Australian tropics (Fig. 1), an area that experiences intense TC- and monsoon-derived rainfall. KNI-51 (15.18°S, 128.37°E, ~100 m elevation) is located in the low-lying Ningbing range of the eastern Kimberley of tropical Western Australia, ~20 km south of the Timor Sea (Fig. 1). The cave consists largely of a single horizontal passage, 600 m in length and accessed by a 2-m<sup>2</sup> entrance located along the valley floor. Clear evidence of flooding is apparent in KNI-51 and includes mud staining on cave walls and speleothems (Fig. 2). Extreme rainfall events flood the cave, suspending fine-grained sediment that coats stalagmite surfaces. Mud layers are encapsulated within these rapidly growing stalagmites after floodwaters recede and growth resumes (31) (Fig. 2). The ages of flood layers, which range in thickness from <1 mm to 10 mm, are tightly bracketed by precise <sup>230</sup>Th dating (typically within ±20 y; 2 SDs) of the stalagmite aragonite. The KNI-51 flood record spans the majority of the last 2,200 y, thereby allowing an examination of the nature of extreme rainfall events across a time span well beyond the reach of direct observation.

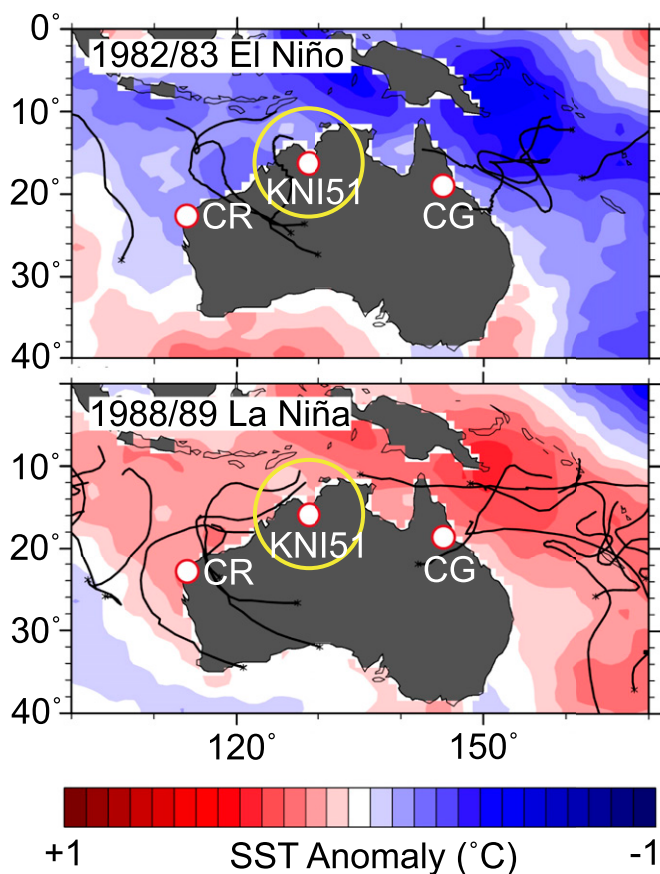


**Fig. 1.** ENSO control of TC activity in the Australian region. (Top) TC tracks (black lines) for the strong El Niño of 1982/1983. Colored contours represent a composite of August–December SST anomalies for all years classified as El Niño during the period 1900–2006; SST anomalies were derived using the classification by ref. 61 that was updated in ref. 62. (Bottom) Same as Top except TC tracks are for the strong La Niña of 1988/1989 and colored contours represent August–December SST anomalies for all years classified as La Niña. Yellow circles denotes 600-km radius from KNI-51; CG, Chillagoe; CR, Cape Range (29). TC track data are from [www.ncdc.noaa.gov/ibtracs/index.php?name=ibtracs-data](http://www.ncdc.noaa.gov/ibtracs/index.php?name=ibtracs-data).

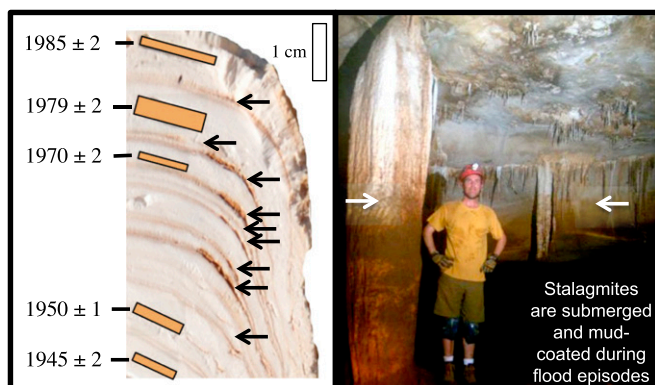


**Fig. 2.** Flood markers in cave KNI-51. (Left) Photograph of slabbed interior of stalagmite KNI-51-11 showing ages and errors of dated intervals (in year CE) and flood layers (black arrows); note preferential preservation of sediment on margins of growth surfaces, likely as a result of erosion of sediment by dripwater striking center of stalagmite cap after floodwaters had receded. Orange rectangles denote positions of dated intervals. (Right) Flood staining in KNI-51 associated predominantly with extreme rainfall events derived from TCs; white arrows denote peak flood level.

The seven stalagmites analyzed in this study were collected from the base of the inclined mud embankment on which they had grown, ~500 m from the entrance; the majority of stalagmites were broken and down when collected (*SI Appendix, Fig. S1*). To calibrate the flood signal, 16 <sup>230</sup>Th dates with errors of ±1–2 y were used to determine the ages of mud layers deposited between the years 1908 CE and 2009 CE in the actively growing sample (KNI-51-11) (*Materials and Methods* and *SI Appendix, Fig. S2* and *Table S1*). Growth was continuous over the last century, but a change in drip position from the center to the margin of the stalagmite in ~1986 CE produced an inclined growth surface that made mud preservation less reliable after this time (*Materials and Methods* and *SI Appendix, Fig. S3*). An additional 33 dates constrain the ages of the six older stalagmites (13), with errors on all stalagmites averaging ±30 y.

The hydroclimate of the Kimberley is dominated by TCs and the Indo-Australian Summer Monsoon (IASM), both of which occur predominantly during austral summer/early fall (December–March) in association with the development of the IASM trough (32). As a result, the region experiences substantial seasonal variability in rainfall, with mean annual precipitation exceeding 800 mm (*SI Appendix, Fig. S4*). Summer rainfall variability is linked to a number of factors, including ENSO (32–35). However, while there is an appeal in the paleoclimate literature for ENSO to have exerted a significant impact on summer precipitation throughout the Australian tropics (13, 36), the influence of ENSO on the monsoon rainfall regime of northwestern Australia is complex. Canonical ENSO events typically have a muted impact on IASM rainfall in this region (33, 37), with La Niña (El Niño) events resulting in only mildly wetter (drier) monsoon seasons. The recently recognized El Niño Modoki may be the exception, with such events seemingly characterized by a shortened monsoon season containing above-average rainfall in some months (38). Rainfall from both TCs and the IASM can be intense, with 1-d totals capable of exceeding 160 mm and maximum 3-d totals approaching 500 mm near KNI-51.

We constrained the precipitation threshold required to flood KNI-51 by comparing daily rainfall data from Carlton Hill Station, the most proximal weather station to the cave site (~40 km), with mud layers in stalagmite KNI-51-11. Carlton Hill Station offers a discontinuous record of daily rainfall data, with the longest gap spanning 1977–1982 CE. Maximum 3-d rainfall accumulations provided the strongest relationship between flood occurrence and rainfall (*P* value < 0.015; *SI Appendix, Figs. S5* and *S6*) and



therefore represent the most likely mechanism for triggering cave flooding. To assess the strength of the link between TCs and precipitation, we examined which of the maximum 3-d rainfall events could be associated with the passage of a TC within a 600-km radius, a window size selected to capture TC rainfall effects (5, 39) (*Materials and Methods* and *SI Appendix*, Fig. S7). Approximately two thirds of extreme rainfall events exceeding 200 mm were related to TCs, while all of the events in excess of 250 mm were TC related (Fig. 3). TCs are similarly responsible for the vast majority of the heaviest 1- and 2-d rainfall events. These numbers are striking considering that observational capabilities were limited before 1970 CE (and thus some TCs likely were not properly identified), and support the notion that TCs are responsible for the majority of heavy rainfall events, and thus flooding, at KNI-51 (Fig. 3). The veracity of the relationship is further supported by similar changes in TC occurrences and cave flood frequencies between 1908 CE and 1986 CE (*SI Appendix*, Fig. S8), although nonstationarity of this relationship may be expected in prehistorical periods.

As a test of the influence of multidecadal changes in the IASM on our record, we compared our flood time series with oxygen isotope variations within the same stalagmites. Oxygen isotopic ratios in monsoon-derived rainwater are largely controlled by the intensity of precipitation events (the so-called “amount effect”) (40), and rainwater derived from TCs can also be anomalously

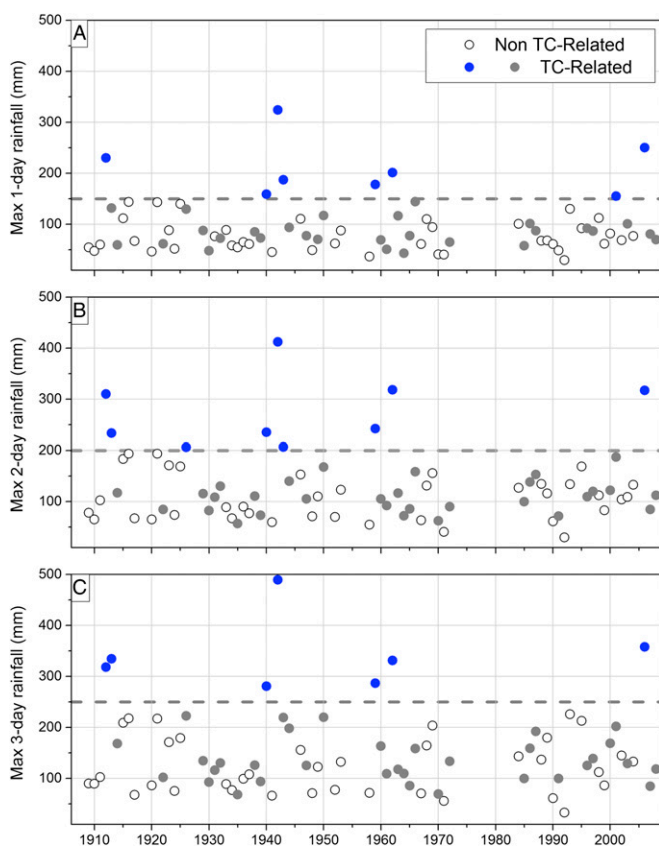


**Fig. 3.** Role of TCs in extreme rainfall events. Peak annual consecutive (A) 1-d, (B) 2-d, and (C) 3-d rainfall totals for Carlton Hill Station for the period of calibration (x axis in years CE). Gaps represent periods of incomplete data collection at the station. Blue and gray circles denote rainfall derived from TCs within a 600-km radius of KNI-51, while white circles denote rainfall associated with events not assigned to TCs. Dashed lines denote the rainfall thresholds exceeded only by TCs (blue circles). TC rainfall varies greatly and depends on storm intensity, distance from the weather station, and duration and track through the area. Thresholds are 150 mm for 1-d, 200 mm for 2-d, and 250 mm for 3-d consecutive events.

depleted in  $^{18}\text{O}$  (41). Infiltrating water from both systems may be preserved within stalagmite carbonate, thereby tracking the strength of the paleomonsoon (13) and, in some cases, past TC activity (26, 29, 42), although extremely high temporal resolution and precise age control are required. Little consistent correspondence is observed between flood events and stalagmite oxygen isotope values, as would be expected if heavy rainfall were simultaneously controlling both oxygen isotope variations and flooding events (*SI Appendix*, Fig. S9). This observation demonstrates that the oxygen isotopic ratios of TC rainfall are poorly coupled to TC frequency at KNI-51, likely due to the fact that the infiltration rate into KNI-51 is rapid, and that stalagmites are routinely submerged (and thus not precipitating aragonite) during extreme rainfall events (*SI Appendix*).

The KNI-51 flood record marks, to our knowledge, the first precisely dated, high-resolution extreme rainfall reconstruction for the central Australian tropics and Indo-Pacific and shows pronounced multicentennial-scale variability. Our record—which, based on these meteorological analyses and monsoon reconstruction, we interpret as largely reflecting TC activity—reveals moderate numbers of extreme rainfall events during 850–1450 CE and 1800–2000 CE and low numbers of extreme rainfall events during 500–850 CE and 1450–1650 CE (no stalagmite was identified that spanned 1650–1750 CE) (Fig. 4). A sharp spike in cave flooding activity at  $\sim 1890$  CE occurs synchronously with the introduction of cattle grazing to the area surrounding KNI-51, and that likely triggered a temporary change in surface hydrology, which may have biased the historical portion of this record (Fig. 4 and *SI Appendix*). The shortest recurrence rates (the highest extreme rainfall activity) and also the greatest variability occurred from 50 CE to 400 CE, with peak values three times those of the 16th century.

### Drivers of Tropical Cyclone Variability

Today, ENSO is recognized as one of the primary drivers of global TC variability, and ENSO impacts the Australian and North Atlantic (including the Caribbean) regions similarly (22, 23). During La Niña years in the instrumental record, both north Australian and North Atlantic TCs are 20% more likely to occur than in El Niño years (21, 43) because cool eastern Pacific sea surface temperature (SST) and steeper zonal Pacific SST gradients during La Niña events enhance low-level atmospheric vorticity in the Atlantic and Australian main development regions while decreasing vertical shear of zonal winds (22, 23, 43) (Fig. 1).

Several studies have examined ENSO as a driver of past TC variability (16, 18–20, 30), but a primary obstacle to understanding the influence of ENSO on prehistoric TCs is the fact that the dynamical nature of ENSO over the late Holocene remains controversial, with no clear consensus yet reached on the timing or sign of ENSO before instrumental records (44–52). Our data provide strong support for the hypothesis that the medieval period (9th through 15th centuries) was characterized by an enhanced La Niña-like climate state in the tropical Pacific Ocean, as has been suggested by numerous previous studies (44, 45, 47–49), explaining the observed elevated TC activity during this time; more El Niño-like conditions characterized much of the 16<sup>th</sup> through 19th centuries, consistent with the reduced TC activity after 1450 CE (Fig. 4).

These trends in Australian TC activity are strikingly similar to those from multiple sites across the North Atlantic and Caribbean basins. Recent reconstructions of Gulf of Mexico (14) and Caribbean (15) hurricanes revealed peak activity during medieval times followed by a sharp decline into the 16<sup>th</sup> through 19th centuries (Fig. 4). A synthesis of TC reconstructions based on eight sites from Puerto Rico and the East Coast of the United States for the last 1,500 y also identified elevated numbers of storms during this time, although significant intrasite variability exists (16) (Fig. 4). Such synchronous shifts between more and less active TC regimes



from the eastern Pacific or Indo-Pacific record enhanced numbers of La Niña events at this time. Thus, addressing this question requires extending accurate, high-resolution ENSO reconstructions from the Pacific basin through the past several millennia.

The influence of ENSO on TC genesis is similar across much of (sub)tropical Australia, including from the western (Cape Range) and northeastern (Chillagoe) portions of the continent (Fig. 1), the sites of recently developed TC reconstructions based on oxygen isotopic ratios in stalagmites (26, 29). The KNI-51 time series differs sharply from these records, with no multicentennial TC variability coincident with either the medieval or 16<sup>th</sup> through 19<sup>th</sup> century periods at Cape Range, and elevated TC activity during the 16<sup>th</sup> through 19<sup>th</sup> centuries in the Chillagoe time series. Today, ENSO impacts cyclogenesis at these sites similarly to the Kimberley (23), and thus the differences between them may reflect climatological origins such as drivers other than ENSO on TC formation or steering (23), rainfall derived from sources other than TCs [i.e., the IASM at KNI-51 and northwest cloud bands at Cape Range (56)], or phenomena such as so-called “masking effects” (57) or kinetic influences on oxygen isotopic values (58)—signals that can be difficult to detect in individual stalagmites; these are important issues that should be addressed in future studies.

Attribution of Australian and Atlantic TC variability to ENSO over the last two millennia serves to refocus attention on the links between a warming world and the tropical Pacific Ocean. Most (22, 59), but not all (2), down-scaled computer models suggest that a decrease in global numbers of TCs will accompany future warming. However, increased greenhouse gas concentrations are likely to shift the heat budget of the western Pacific, which could favor enhanced cyclogenesis if not counteracted by a dynamical response to more El Niño-like conditions. Should the Pacific Ocean transition to a more El Niño-like climate state, as suggested by some model results (24), then less frequent TCs may become the norm over coming decades to centuries. ENSO modulation of extreme rainfall events—largely through TCs but also through less pronounced impacts on the IASM—should be considered in hydroclimate models of the Indo-Pacific.

## Materials and Methods

**Flood Layer Analysis.** Each KNI-51 stalagmite was bisected along its vertical growth axis using a water-cooled rock saw. Accumulations of mud layers, ranging in height from <1 mm to 10 mm, drape numerous growth horizons throughout each sample. The position of flood layers was measured to the nearest half-millimeter from the base of the stalagmite and fitted to the growth model derived from the <sup>230</sup>Th dates. This growth model was adjusted to account only for the deposition of stalagmite carbonate and is not distorted by the thickness of individual mud layers. Preservation and detection of flood-derived mud layers in stalagmites is subject to several caveats. First, as they grow, stalagmites require increasingly deep floodwaters to deposit mud on their caps. Second, mud deposits form a zone of structural weakness within a stalagmite that could be eroded by later floods, erasing evidence of previous storm events. Third, the geometry of individual stalagmites impacts their ability to preserve mud layers. Angular tops on thin stalagmites or steeply inclined tops form the least suitable geometries to preserve sediment deposited by flooding. In many cases, mud layers were most visible on the cap margins, suggesting that some sediment was eroded by dripwater before crystallization of aragonite. Because of this fact, the position in which each stalagmite was bisected introduced some degree of variability into our ability to recognize and classify mud layers. The majority of stalagmites were broken and down when collected at the base of the mud bank on which they grew, 1–2 m below recent flood markers preserved on the cave walls. We attempted to address these potential problems by using stalagmites formed below the height of cave flood markers, by obtaining a high number of precise radiometric dates, particularly during the twentieth century, the period of calibration, and, wherever possible, by constructing time series from multiple, coeval stalagmites.

Mud layers were assigned to one of four categories, depending on the maximum defined thickness of mud accumulation: Type 1, <0.5 mm; Type 2, 0.5–1.0 mm; and Type 3, >1.0 mm (SI Appendix, Fig. S10). Numerous stains on stalagmite growth surfaces are also present (designated as Type 0), but

since no appreciable mud accumulation is apparent in these layers, they cannot be interpreted unambiguously as resulting from cave flooding events and thus were not included in our record. However, including Type 0 events in the time series resulted in an increase in the frequency of cave flooding events but largely maintained the overall patterns (SI Appendix, Fig. S11). The distribution of these types varied between stalagmites, in part because differentiation between flood types is to some degree subjective and includes the biases associated with preservation. Sample KNI-51-10 is somewhat unusual in that it is characterized exclusively by Type 1 (and Type 0) events. The fine-scale interlayering of flood layers in this sample is responsible for the markedly lower precision on its <sup>230</sup>Th dates relative to the other stalagmites.

Identifying biases within individual stalagmites marks an important step in assessing their utility as paleostorm indicators (31). The flood records from coeval stalagmites reveal similar variability at multidecadal scales; the only exception is KNI-51-G (1340–1640 CE), which records flood occurrence rates marginally higher than those observed in the two other stalagmites of similar age, although short-term and long-term trends in flood activity are nearly identical (SI Appendix, Fig. S12). The origin of this discrepancy is unclear but may be related to biases associated with flood layer preservation or identification, or the elevation at which this stalagmite grew on the mud bank.

**<sup>230</sup>Th Dating.** Samples for dating were milled by a hand-held Dremel tool or by using a computer-guided drill with either a 1- or 2-mm-diameter bit. Radioisotopic ages were obtained with <sup>238</sup>U-<sup>234</sup>U-<sup>230</sup>Th disequilibrium techniques at the University of New Mexico, and ages of mud layers were determined by polynomials fit to dated intervals. Approximately 50–100 mg of aragonite was milled from each interval of interest and then dissolved, spiked with a mixed <sup>229</sup>Th-<sup>233</sup>U-<sup>236</sup>U tracer, and processed using column chemistry methods. The U and Th fractions were dissolved in a 3% HNO<sub>3</sub> 4-mL solution, which was then aspirated into a Thermo Neptune multi-collector inductively-coupled plasma mass spectrometer using a Cetac Aridus II low flow (50–100 μL/min) desolvating nebulizer system. U and Th separates were run as static routines where all isotopes were measured in Faraday cups, with the exception of <sup>230</sup>Th, which was measured using the secondary electron multiplier (SEM). Gains between the SEM and Faraday cups were determined using standard solutions of NBL-112 for U and an in-house <sup>230</sup>Th-<sup>229</sup>Th standard for Th, both of which were measured routinely. U and Th blanks are <20 pg, and half-lives of <sup>230</sup>Th and <sup>234</sup>U are those of ref. 60. Unsupported <sup>230</sup>Th was corrected for using an initial <sup>230</sup>Th/<sup>232</sup>Th ratio equal to the average crustal silicate value of  $4.4 \times 10^{-6}$  (±50%). Because <sup>232</sup>Th concentrations were very low, the ages of the uncorrected and detrital Th-corrected ages were nearly identical. Elevated U abundances and δ<sup>234</sup>U values, low detrital Th (<sup>232</sup>Th) concentrations, and high growth rates allowed extremely precise age determinations on samples as young as 1 y old (SI Appendix, Table S1).

**Calibrating the KNI-51 Flood Record.** Considering only those years containing complete wet season rainfall data (December–March), the stalagmite and rainfall time series overlapped for a total of 66 y between 1908 CE and 2008 CE. We calculated 1-, 2-, and 3-d maximum rainfall totals over the December–March period and compared these data to the KNI-51-11 flood layer time series. Flood events were assigned to individual years, and a best-case correspondence was calculated by shifting the mud layer ages by up to ±1 y (the minimum age model uncertainties) to maximize their fit to these peak rainfall events, thereby preserving the temporal continuity of the mud layers. This is a somewhat conservative method, given that it does not allow for compression or expansion of ages for consecutive flood layer events, even if it were possible within the errors of the dates to do so while still maintaining stratigraphic superposition. Because of the binary nature of the data (occurrence or nonoccurrence of a flood event), we used logistic regression to examine the relationship between extreme rainfall and flood events. Our expectation is that the larger the rainfall amount, the higher the probability of flooding (SI Appendix, Fig. S6).

**ACKNOWLEDGMENTS.** This manuscript benefited greatly from comments by editor Kerry A. Emanuel and three anonymous reviewers. We thank Donna Cavlovic for assistance at KNI-51 and in Kununurra. Funding was provided by the Paleo Perspectives on Climate Change program of the US National Science Foundation (NSF) through Grant AGS-1103413, a seed grant from the Center for Global and Regional Environmental Research, and Cornell College (all to R.F.D.), the Kimberley Foundation Australia (to K.-H.W.), and Penzance and John P. Chase Memorial Endowed Funds at Woods Hole Oceanographic Institution (to C.C.U.). Yemane Asmerom, V.J.P., and the Radiogenic Isotope Laboratory at the University of New Mexico supported much of the chronology work through NSF ATM-0703353 and EAR-0326902.



1. Li X-F, Yu J, Li Y (2013) Recent summer rainfall increase and surface cooling over Northern Australia since the late 1970s: A response to warming in the Tropical Western Pacific. *J Clim* 26:7221–7239.
2. Emanuel KA (2013) Downscaling CMIP5 climate models shows increased tropical cyclone activity over the 21st century. *Proc Natl Acad Sci USA* 110(30):12219–12224.
3. Kossin JP, Emanuel KA, Vecchi GA (2014) The poleward migration of the location of tropical cyclone maximum intensity. *Nature* 509(7500):349–352.
4. Emanuel K (2005) Increasing destructiveness of tropical cyclones over the past 30 years. *Nature* 436(7051):686–688.
5. Dare R, Davidson N, McBride J (2012) Tropical cyclone contribution to rainfall over Australia. *Mon Weather Rev* 140:3606–3619.
6. Mei W, Primeau F, McWilliams J, Pasquero C (2013) Sea surface height evidence for long-term warming effects of tropical cyclone on the ocean. *Proc Natl Acad Sci USA* 110(38):15207–15210.
7. Wyrwoll K-H, Miller G (2001) Initiation of the Australian summer monsoon 14,000 years ago. *Quat Int* 83-85:119–128.
8. Russell JM, Johnson TC (2007) Little Ice Age drought in equatorial Africa: Intertropical convergence zone migrations and El Niño–Southern Oscillation variability. *Geology* 35(1):21–24.
9. Tierney J, Oppo D, Rosenthal Y, Russell J, Linsley B (2010) Coordinated hydrological regimes in the Indo-Pacific region during the past two millennia. *Paleoceanography* 25(1):PA1102.
10. Mohtadi M, et al. (2011) Glacial to Holocene swings of the Australian-Indonesian monsoon. *Nat Geosci* 4:540–544.
11. Zhang P, et al. (2008) A test of climate, sun, and culture relationships from an 1810-year Chinese cave record. *Science* 322(5903):940–942.
12. Griffiths M, et al. (2009) Increasing Australian-Indonesian monsoon rainfall linked to early Holocene sea-level rise. *Nat Geosci* 2:636–639.
13. Denniston R, et al. (2013) A stalagmite record of Holocene Indonesian–Australian summer monsoon variability from the Australian tropics. *Quat Sci Rev* 78:155–168.
14. Lane P, Donnelly J, Woodruff J, Hawkes A (2011) A decadal-resolved paleohurricane record archived in the late Holocene sediments of a Florida sinkhole. *Mar Geol* 287:14–30.
15. Denomnee KC, Bentley SJ, Droxler AW (2014) Climatic controls on hurricane patterns: A 1200-y near-annual record from Lighthouse Reef, Belize. *Sci Rep* 4:3876.
16. Mann ME, Woodruff JD, Donnelly JP, Zhang Z (2009) Atlantic hurricanes and climate over the past 1,500 years. *Nature* 460(7257):880–883.
17. Scileppi E, Donnelly J (2007) Sedimentary evidence of hurricane strikes in western Long Island, New York. *Geochem Geophys Geosyst* 8(6):Q06011.
18. Donnelly JP, Woodruff JD (2007) Intense hurricane activity over the past 5,000 years controlled by El Niño and the West African monsoon. *Nature* 447(7143):465–468.
19. Woodruff J, Donnelly J, Mohrig D, Geyer W (2008) Reconstructing relative flooding intensities responsible for hurricane-induced deposits from Laguna Playa Grande, Vieques, Puerto Rico. *Geology* 36(5):391–394.
20. Nott J, Forsythe A (2012) Punctuated global tropical cyclone activity over the past 5,000 years. *Geophys Res Lett* 39:L14703.
21. Kuleshov Y (2012) Southern Hemisphere tropical cyclone climatology. *Modern Climatology*, ed Wang S-Y (InTech, Rijeka, Croatia).
22. Camargo S, Emanuel K, Sobel A (2007) Use of a Genesis Potential Index to diagnose ENSO effects on tropical cyclone genesis. *J Clim* 20:4819–4834.
23. Ramsay H, Camargo S, Kim D (2012) Cluster analysis of tropical cyclone tracks in the Southern Hemisphere. *Clim Dyn* 39:897–917.
24. Vecchi G, Soden B (2007) Global warming and the weakening of the tropical circulation. *J Clim* 20:4316–4340.
25. Collins M, et al. (2010) The impact of global warming on the tropical Pacific Ocean and El Niño. *Nat Geosci* 3:391–397.
26. Nott J, Haig J, Neil H, Gillieson D (2007) Greater frequency variability of landfalling tropical cyclones at centennial compared to seasonal and decadal scales. *Earth Planet Sci Lett* 355:367–372.
27. Nott J (2011) A 6000 year tropical cyclone record from Western Australia. *Quat Sci Rev* 30:713–722.
28. Toomey M, Donnelly J, Woodruff J (2013) Reconstructing mid-late Holocene cyclone variability in the Central Pacific using sedimentary records from Tahaa, French Polynesia. *Quat Sci Rev* 77:181–189.
29. Haig J, Nott J, Reichert G-J (2014) Australian tropical cyclone activity lower than at any time over the past 550–1,500 years. *Nature* 505(7485):667–671.
30. Woodruff J, Donnelly J, Okuso A (2009) Exploring typhoon variability over the mid-to-late Holocene: Evidence of extreme coastal flooding from Kamikoshiki, Japan. *Quat Sci Rev* 28:1774–1785.
31. Frappier A, et al. (2014) Two millennia of tropical cyclone-induced mud layers in a northern Yucatán stalagmite reveal: Multiple overlapping climatic hazards during the Maya Terminal Classic “megadroughts”. *Geophys Res Lett* 41(14):5148–5157.
32. Suppiah R (1992) The Australian summer monsoon: A review. *Prog Phys Geogr* 16:263–318.
33. Wheeler M, McBride J (2011) Australasian monsoon. *Intraseasonal Variability in the Atmosphere–Ocean Climate System*, eds Lau WKM, Waliser DE (Springer, New York), 2nd Ed, pp 147–198.
34. Taschetto A, England M (2009) An analysis of late twentieth century trends in Australian rainfall. *Int J Climatol* 29:791–807.
35. Risbey J, Pook M, McIntosh P, Wheeler M, Hendon H (2009) On the remote drivers of rainfall variability in Australia. *Mon Weather Rev* 137:3233–3253.
36. McGowan H, Marx S, Moss P, Hammond A (2012) Evidence of ENSO mega-drought triggered collapse of prehistory Aboriginal society in northwest Australia. *Geophys Res Lett* 39(22):L22702.
37. McBride J, Nicholls N (1983) Seasonal relationships between Australian rainfall and the Southern Oscillation. *Mon Weather Rev* 111:1998–2004.
38. Taschetto A, et al. (2010) Australian monsoon variability driven by a Gill–Matsuno type response to central-west Pacific warming. *J Clim* 23:4717–4736.
39. Villarini G, et al. (2014) Sensitivity of tropical cyclone rainfall to idealized global scale forcings. *J Clim* 27:4622–4641.
40. Lachniet M (2009) Climatic and environmental controls on speleothem oxygen isotope values. *Quat Sci Rev* 28:412–432.
41. Lawrence J, Gedzelman S (1996) Low stable isotope ratios of tropical cyclone rains. *Geophys Res Lett* 23:527–530.
42. Frappier AB, Sahagian D, Carpenter SJ, González LA, Frappier BR (2007) Stalagmite stable isotope record of recent tropical cyclone events. *Geology* 35(2):111–114.
43. Klotzbach P (2011) El Niño–Southern Oscillation’s impact on Atlantic basin hurricanes and U.S. landfalls. *J Clim* 24:1252–1263.
44. Makou MC, Eglinton TL, Oppo DW, Hughen KA (2010) Postglacial changes in El Niño and La Niña behavior. *Geology* 38(1):43–46.
45. Cobb KM, Charles CD, Cheng H, Edwards RL (2003) El Niño/Southern Oscillation and tropical Pacific climate during the last millennium. *Nature* 424(6946):271–276.
46. Conroy JL, Overpeck JT, Cole JE (2010) El Niño/Southern Oscillation and changes in the zonal gradient of tropical Pacific sea surface temperature over the last 1.2 ka. *PAGES News* 18:32–34.
47. Mann ME, et al. (2009) Global signatures and dynamical origins of the Little Ice Age and Medieval Climate Anomaly. *Science* 326(5957):1256–1260.
48. Khider D, Stott L, Emile-Geay J, Thunell R, Hammond D (2011) Assessing El Niño Southern Oscillation variability during the past millennium. *Paleoceanography* 26(3):PA3222.
49. Seager R, et al. (2008) Tropical Pacific forcing of North American Medieval megadroughts: Testing the concept with an atmospheric model forced by coral-reconstructed SST. *J Clim* 21(23):6175–6190.
50. Moy CM, Seltzer GO, Rodbell DT, Anderson DM (2002) Variability of El Niño/Southern Oscillation activity at millennial timescales during the Holocene epoch. *Nature* 420(6912):162–165.
51. Yan H, et al. (2011) A record of the Southern Oscillation index for the past 2,000 years from precipitation proxies. *Nat Geosci* 4:611–614.
52. Newton A, Thunell R, Stott L (2011) Changes in the Indonesian Throughflow during the past 2000 yr. *Geology* 39(1):63–66.
53. Hall J, Matthews A, Karoly D (2001) The modulation of tropical cyclone activity in the Australian region by the Madden–Julian Oscillation. *Mon Weather Rev* 129:2970–2982.
54. Klotzbach P (2010) On the Madden–Julian–Atlantic hurricane relationship. *J Clim* 23:282–293.
55. Goodwin I, et al. (2014) A reconstruction of extratropical Indo-Pacific sea-level pressure patterns during the Medieval Climate Anomaly. *Clim Dyn* 43:1197–1219.
56. Telcik N, Pattiaratchi C (2014) Influence of northwest cloudbands on southwest Australian rainfall. *J Climatol* 2014:671394.
57. Frappier A (2013) Masking of inter-annual climate proxy signals by residual tropical cyclone rainwater: Evidence and challenges for low-latitude speleothem paleoclimatology. *Geochem Geophys Geosyst* 14:3632–3647.
58. Mickler P, et al. (2004) Stable isotope variations in modern tropical speleothems: Evaluating equilibrium vs. kinetic isotope effects. *Geochim Cosmochim Acta* 68:4381–4393.
59. Knutson T, et al. (2010) Tropical cyclones and climate change. *Nat Geosci* 3:157–163.
60. Cheng H, et al. (2013) Improvements in  $^{230}\text{Th}$  dating,  $^{230}\text{Th}$  and  $^{234}\text{U}$  half-life values, and U-Th isotopic measurements by multi-collector inductively coupled plasma mass spectrometry. *Earth Planet Sci Lett* 371-372:82–91.
61. Meyers G, McIntosh P, Pigot L, Pook M (2007) The years of El Niño, La Niña, and interactions with the tropical Indian Ocean. *J Clim* 20:2872–2880.
62. Ummenhofer CC, et al. (2009) What causes southeast Australia’s worst droughts? *Geophys Res Lett* 36(4):L04706.